Nanoscale

Accepted Manuscript

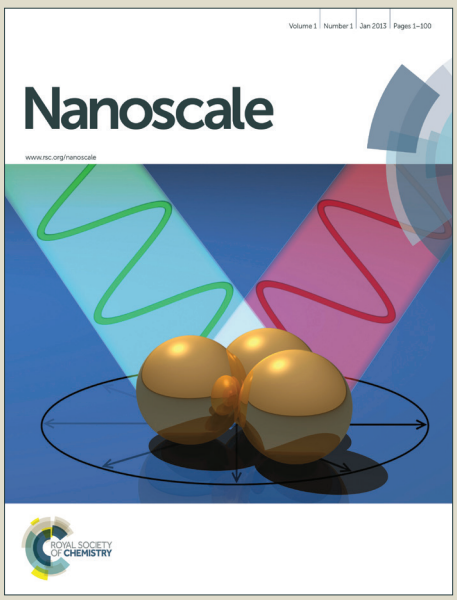

ROYAL SOCIETY OF CHEMISTRY

www.rsc.org/nanoscale

ARTICLE TYPE www. rsc.org/xxxxxx | XXXXXXXX

Electrically Driven Plasmon Mediated Energy Transfer between ZnO Micrcowire and Au Nanoparticles

Bin Zhao,[a,b] Ming-Ming Jiang,[a] Dong-Xu Zhao,*[a] Yang Li,[a] Fei Wang,[a] and De-Zhen Shen[a]

Received Xth XXXXXXXXXX 20XX, Accepted Xth XXXXXXXXX 20XX
First published on the web Xth XXXXXXXXXX 200X
DOI: 10.1039/b000000x

Electrically driven energy transfer between the surface defect states of ZnO quadrilateral microwires (MWs) and localized surface plasmon polaritons has been realized by means of introducing Au nanoparticles (NPs). A electroluminescence device with green emitting using ZnO quadrilateral MWs, was fabricated. Once the Au NPs sputtered on the surfaces of ZnO MWs, electroluminescence of ZnO MWs will shift from green to red. Meanwhile, dual emissions have been observed by means of sputtering Au NPs on a single ZnO MW periodically. Due to the Au NPs, electrically driven plasmon mediated energy transfer can achieve the modulation of amplifying, or quenching the surface defects emission. The relevant dynamic process of the surface plasmon modes mediated energy transfer has been investigated. This new energy transfer method potentially offers an approach of modification and recombination on the surface defect states excitations of wide bandgap semiconductor materials.

1 Introduction

Energy transfer process involving the excitation energy from excited donor semiconductor nano/micro-structures transfer to metal nanostructures is of critical importance for the emerging field of plasmon-enhanced metal photoluminescence and plays an important role in diverse phenomena across physics, chemistry, and biology[1–8]. Examples include effective transfer of excitation energy from donor molecules to acceptor molecules on opposite sides of metal films supported by coupled surface plasmon polaritons (SPPs)[9,10]. This variant of SPPs mediating radiative transfer should allow directional control over the flow of excitation energy with the use of suitably designed metallic nanostructures. Comparing with nonradiative energy transfer (such as F*ö*rster Energy Transfer), radiative energy transfer has sufficient distance range but poor efficiency and directionality. The surface plasmons of the exquisitely designing and optimizing metal nanostructures are powerful tools to enhance the efficiency of both radiative and nonradiative energy transfers[11–15].

Excitation energy transfer from donor to acceptor could be simply divided into two broad categories: radiative transfer, and nonradiative transfer. In contrast with nonradiative transfer, radiative transfer, is a simple emission and absorption process. Radiative recombination in gold, copper, and gold-copper alloys has been observed arising from transitions between electrons in conduction-band states below the Fermi level and holes in the *d* bands generated by optical excitation[16–19]. Metal photoluminescence (PL) originates from radiative recombination of photoexcited core holes and conduction band electrons, and can be enhanced due to the surface plasmon local field effect[20]. In addition to producing strong localized electric fields, resonant plasmons in noble metal nanostructures are also responsible for the absorption of photons to create excited or hot electrons in the metal. Interestingly, the inverse process, namely, of generating photons from non-equilibrium electrons in metal nanostructures themselves, can be facilitated by resonant plasmons, as well. Consequently, PL in gold nanoparticles has been ascribed to the radiative damping of particle plasmons generated by the recombination of *sp* band electrons and excited *d* band holes[11,18].

In contrast with conventional light sources, light-emitting diodes on the basis of wide bandgap semiconductor materials, such as ZnO, GaN, are becoming the alternative for future general lighting applications owing to their high efficiency and reliability[21,22]. The broad visible emission observed in ZnO has been attributed variously to interstitial zinc ions Zn_i, oxygen vancancies V_O, chemisorbed oxygen, divalent copper impurities, and zinc vacancies V_{Zn}. Presently, V_O is thought to be the likely cause of the visible emission around 500 nm[23–31]. Nevertheless, reports on the electroluminescence (EL) of surface defects are very rare[31,32]. Plasmon enhanced band emission of ZnO has been achieved by the deposition of metals such as Ag, Au, Al, and Pt on ZnO films, as a result of the resonant coupling between the surface plasmon of metal and the band gap emission of ZnO[8,32–37]. The quenching of exciton emission in semiconducting micro/nano-structures

[a] *State key Laboratory of Luminescence and Applications, Changchun Institute of Optics, Fine Mechanics and Physics, Chinese Academy of Sciences, No.3888 Dongnanhu Road, Changchun, 130033, People's Republic of China.*
[b] *University of the Chinese Academy of Sciences, Beijing, 100049, People's Republic of China.*
* *E-mail: zhaodx@ciomp.ac.cn.*

by fluorophores has been studied extensively over the past decade [5,38,39]. Previous reports have focused overwhelmingly on energy transfer from the exciton state of the micro/nano-structures [1,2,8]. To date, there have been no systematic studies of energy transfer from charge carriers in defect or trap states of micro/nano-structures to acceptors [34,40,41]. Such studies are important that surface defect states recombination limits the overall radiative quantum yield of the semiconductor micro/nano-structures. In some cases, the defect emission may even dominate over exciton emission.

However, some doubts remain in the involvement of plasmons in the EL process on the basis of bandgap semiconductor nano/micro-structures, and an agreement in a mechanism for the EL process in nanostructures is lacking [35,38–42]. Electrically driven excitation energy transfer from donor to acceptor is a rarely researched field, which should be given further attention. In this paper, detailed experimental and theoretical studies of the energy transfer from the defect states of ZnO microwires to the Au NPs were present. The visible defect emission of bare ZnO microwires were studied under electrically driven. By means of introducing Au NPs, Au dimers localized surface plasmon resonances around 600 nm were demonstrated. Meanwhile, surface defects luminescence were suppressed and the luminescence center then transferred from 500 nm to 600 nm, which originated from radiative recombination of photoexcited localized surface plasmon resonances. The energy transfer process involving the interaction between surface defect states and surface plasmons were taken into account. In addition, Au NPs were sputtered periodically on a single ZnO microwire, dual emissions fluorescence around 500 nm and 600 nm can be observed simultaneously.

2 Experimental section

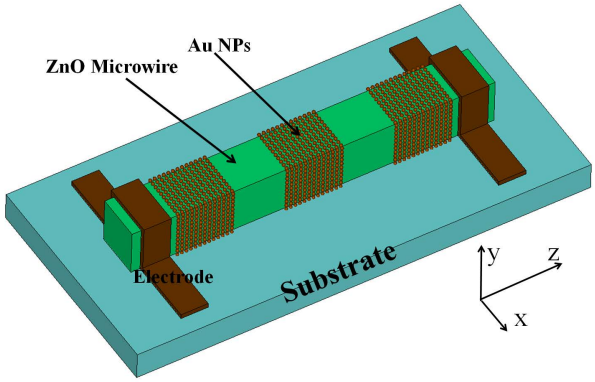

Fig. 1 Schematic diagram of electrically driven electroluminescence devices consisting of ZnO microwire and Au NPs.

The ZnO microwires were synthesised via a traditional chemical vapour deposition method in a horizontal tube furnace at 1000 °C. Glass substrates were cut into pieces of 1 cm × 1 cm, and strictly ultrasonic cleaned in acetone, ethanol and deionized water separately, 15 minutes for each. Subsequently, a ZnO microwire was selected to put on the substrates. Two Indium (In) particles were put on the two ends of ZnO MW as the electrodes. After a 400 °C annealing of 2 minutes, ZnO MW can be fixed on the substrate. Then metal-semiconductor-metal (MSM) structure based EL devices was fabricated. The Au nanoparticles was deposited on the surfaces of the ZnO MWs by a radio-frequency magnetron sputtering technique at room temperature with the pressure of 5×10^{-2} Pa, then the localized surface plasmons (LSPs) enhanced MSM structure EL devices were fabricated.

The morphology of the ZnO MWs and Au NPs were characterized by field-emission scanning electron microscopy (FESEM) (model: Hitachi S-4800). The current-voltage (I-V) characteristics of the devices were measured using a keithley 2611 system. The PL measurements of ZnO MWs were performed using a He-Cd laser line of excitation wavelength 325 nm, and a micro-Raman spectrometer in a backscattering geometry configuration, which used to detect the emission spectra (model: LABRAM-UV Jobin Yvon), can focus on an area of diameter 10 μm and adjust the depth of the lasing focus. The fluorescence measurements of Au NPs were performed using a xenon lamp of excitation wavelength of 500 nm in a Hitachi F7000 fluorescence spectrophotometer. The EL spectra of the device were performed in a Hitachi F4500 spectrometer. The EL phenomenons can be observed, as well as the corresponding EL spectra collecting of the device placed in a optical microscope. The absorption spectra were carried out using a Shimadzu UV-3101 PC spectrophotometer.

3 Results and discussion

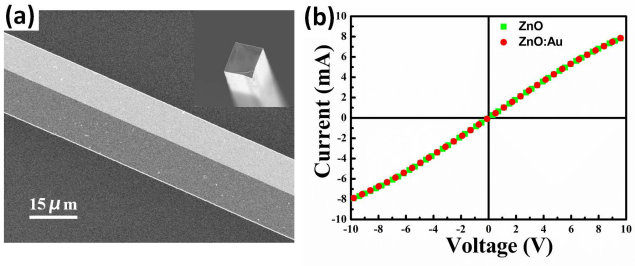

Fig. 2 Physical characteristics: (a) SEM images of single ZnO microwire on silicon substrate directed along the polar *c*-axis exhibiting a quadrilateral crystal symmetry, the inset shows the quadrilateral cross section; (b) exhibits I-V characteristics of bare ZnO MWs based EL devices, and Au NPs coated ZnO MWs based EL devices.

Schematic diagram of ZnO based metal semiconductor metal (MSM) devices is shown in Fig. 1, in which the ZnO microwire is modified by means of introducing Au NPs on the outside surfaces periodically. A typical SEM image of ZnO MW is shown in Fig. 2(a). The diameters of ZnO MWs is about 10-15 μm and lengths of 1-2 cm. The inset indicates that ZnO MWs possess quadrilateral cross-section. Figure 2 (b) shows the I-V characteristics of the MSM device together with the Au NPs overclothes. The I-V curve presents a linear relationship, which indicates the formation of the Ohmic contacts of ZnO MWs. After introducing the Au NPs, the I-V characteristics has no changes, indicating that the Au NPs have no influence on the resistance of ZnO MWs.

Figure 3(a) illustrates the EL of a bare ZnO microwire, in which the spectra center located at 500 nm under different injection currents. The inset shows highlight green emitting with a camera. Figure 3(b) shows the EL of the ZnO microwire modified with Au nanoparticles, in which the luminescence center located around 600 nm under different injection current. The inset shows highlight red emitting with a camera. Therefore, owing to the introduction of Au NPs, obvious shift of luminous center occurs ranged from 500 nm to 600 nm. According to the Fig. 3, it is obvious that the introduction of the Au NPs can be used to modulate the luminescence center of ZnO MWs, meanwhile, the suppression of the green emission can also be obtained. Previous studies have demonstrated that ZnO PL is sensitive to the presence of various adsorbates such as O_2, H_2, CO, and metal NPs[23,27,28,43]; however, few related reports on the EL mechanism, as well as the shift of luminescence centers on account of ZnO microwire were demonstrated[32,44].

In order to confirm the origin of the EL emission, PL measurements were performed. Figure 4(a) demonstrates that there is a strong broad visible emission located at 500 nm consistent with the EL spectra, which is corresponding to the oxygen vacancies (V_O) defects of ZnO in previous reports[23–28]. While internal photoemission by means of keeping the pumped light focusing inside of the measured ZnO MW, the PL spectrum shown in Fig. 4(b) demonstrates that there is only an ultraviolet (UV) emission located at 387 nm, corresponding to the near-band-edge emission. Oxygen vacancies V_O are the most widely accepted mechanism for the visible emission of ZnO, they can occur in three charge states: the doubly ionized oxygen vacancy V_O^{++} which does not capture any electrons and is doubly positive charged relative to the lattice of ZnO, the singly ionized oxygen vacancy V_O^{+} which has captured one electron and is singly positive charged relative to the lattice, the neutral oxygen vacancy V_O^{x}[23,24,27,43]. According to the levels of these three oxygen vacancies in the energy band of ZnO, the origin of the green emitting peaks can be attributed to the electron transition from V_O^{+} centers to the valence band edge. In atmospheric environment, oxygen molecules could

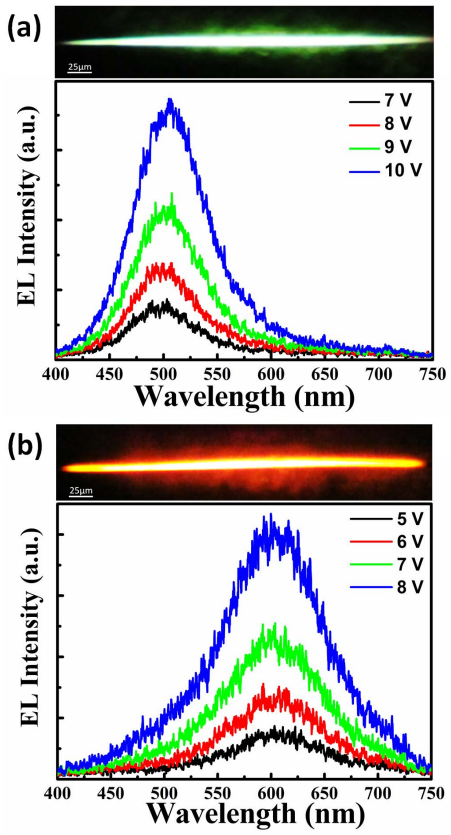

Fig. 3 Luminescence spectra under electrical driven: (a) shows the EL spectra of a bare ZnO MW operated from 7 V to 10 V, the inset demonstrates the camera images corresponding to the EL pattern (green) along the MW length direction; (b) displays EL spectra of Au NPs coated ZnO MW operated from 5 V to 8 V, the inset demonstrates the camera images corresponding to the EL pattern (red) along the MW length direction.

be absorbed on the surfaces of ZnO MWs then trapped free electrons $\left[O_2 + e^- \rightarrow O_2^-\right]$, thus create a thin depletion layers near the surfaces[45]. The sketch of energy band is shown in Fig. 4(c), which shows a depletion layer within the surfaces of ZnO MWs. Free electrons are supplied by oxygen vacancies (V_O) $\left[V_O - e^- \rightarrow V_O^+\right]$. There is a large number of V_O^+ defects existing within the surface depletion layers of ZnO MWs, which has been confirmed by the PL measurements. A model based on the inelastic scattering of tunneling electrons has been proposed for the EL emissions from the ZnO MWs based MSM devices according to the previous report of our group[46]. The electrons under a high bias voltage have sufficient energy to scatter inelastically and then tunneling through the depletion layer to excite the defect states. In terms of comprehensive, the green emitting of EL is caused by the electron transition from V_O^+ centers to the valence band edge near the surfaces of ZnO MWs.

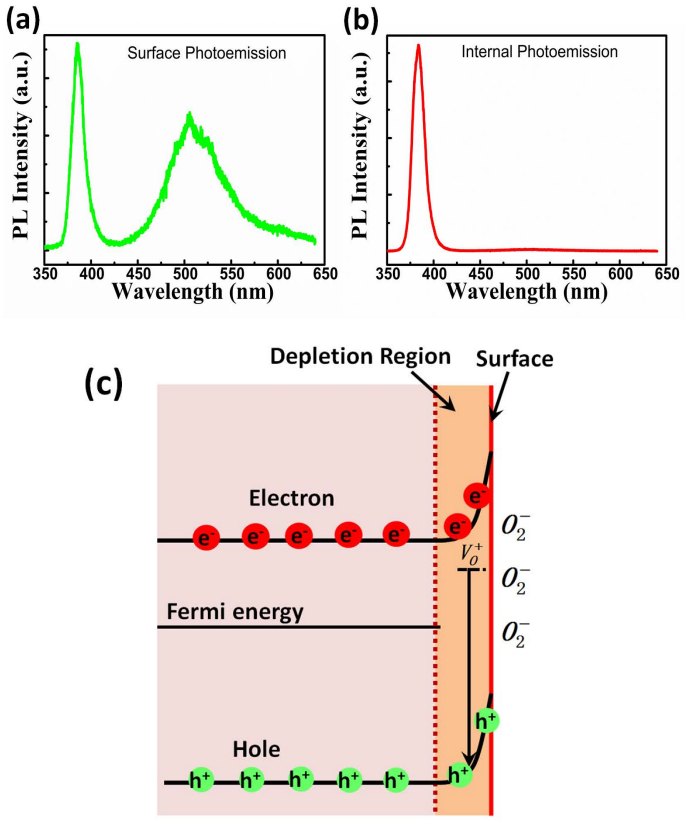

Fig. 4 Surface defect luminescence of bare ZnO MWs: (a) Surface photoemission by means of keeping the pumping light focusing on the measured surface of ZnO MW, which show the surface defects luminescence center around 500 nm; (b) Internal photoemission by means of keeping the pumped light focusing inside of the measured ZnO MW, in which the defect luminescence can not be observed; (c) Sketch of the energy band of the ZnO MW with the surface defect modes and corresponding the surface depletion region, ZnO MWs possess high electron concentration, as well as a surface depletion region with small width, V_O^+ defect modes exists in the depletion region, the Fermi level is lower than the V_O^+ surface defect level, and almost the V_O^+ are fulfilled.

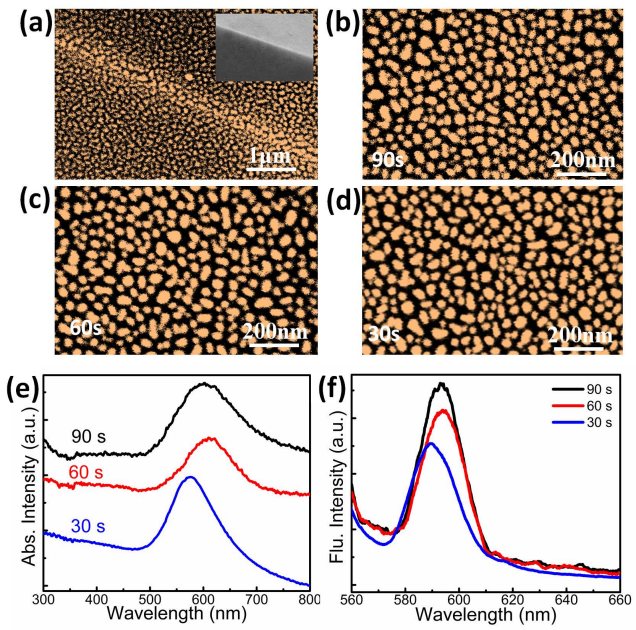

Fig. 5 (a) demonstrates the SEM image of Au nanoparticles coated ZnO MW, the inset showing its corresponding bare ZnO microwire; (b)-(d) demonstrated SEM images of Au nanoparticles, with its corresponding sputtering time; (e) demonstrates corresponding absorption (Abs) spectra; (f) demonstrates the corresponding fluorescence (Flu.) spectra of Au nanoparticles with the excitation of 500 nm.

Taken the influence of Au nanoparticles on the luminescence into account, the absorption spectra of the Au nanoparticles were carried out. Figures 5(a)-(d) demonstrate the SEM images of Au nanoparticles coated ZnO microwire. Figure 5(a) displays the overall SEM images of Au NPs coated ZnO MWs, the inset showing its corresponding bare ZnO MW. Therefore, ZnO MWs have been coated by Au NPs completely. Figures. 5(b)-(d) demonstrates the SEM images with different sputtering times, such as 30 s, 60 s, and 90 s. The absorption spectra demonstrated in Fig. 5(e) indicate that there is a strong absorption peak around 600 nm. Therefore, the preparation of the random distribution of Au NPs could be used to excite dipole surface plasmon resonances around 600 nm[9,16,17,47,48]. The shift and intensities of localized surface plasmon resonances can be derived from the densities of Au NPs. The fluorescence spectra of Au nanoparticles with different sputtering times is shown in Fig. 5(f), in which the luminescence center located around 600 nm with the help of a excitation source of 500 nm. Together with the absorption peak of Au nanoparticles around 600 nm shown in Fig. 5(e), absorption peak around 600 nm can be responsible for the localized surface plasmon resonances of Au NPs. It means that Au NPs plasmons mediated can be used to implement the amplification of EL around 600 nm of ZnO microwire. Detailed plasmon mediated transfer process will be described below.

According to the SEM images shown in Figs. 5(a)-(d), the diameter of Au NPs around D = 60 nm and the gap distance g ranged from 5 nm to 30 nm can be obtained. In consequence, the extinction spectra of Au NPs and corresponding field distributions can be carried out by means of the time domain and frequency domain (FDTD) finite element methods[49,50]. In the calculation and simulation processes, the refractive index of the particles' environment was assumed to be n_e = 1.7, the electromagnetic field was linearly polarized along a fixed interparticle axis. To approximate the experimental illumina-

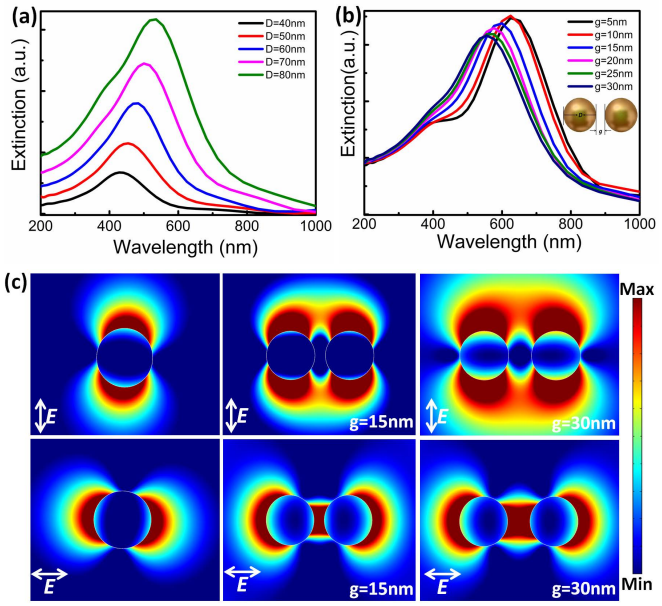

Fig. 6 Extinction spectra and field distribution of Au NPs: (a) demonstrates the extinction spectra of a isolated Au nanoparticle, with the diameter ranged from 40 nm to 80 nm; (b) demonstrates the extinction spectra of a dimer of Au NPs, with the diameter $D = 60$ nm, and the gap distances g ranged from 5 nm to 30 nm; (c) displays the corresponding electric field distribution, with the parameter of $D = 60$ nm, and the gap distances shown in the inset, the resonance wavelength simulated can be referred to the extinction spectra with the Au optical constants can be referred to Ref[49].

tion conditions, the plasmon shift versus interparticle separation relationship by averaging over a wide range of incident wave vectors and light polarizations were taken into account. Fig. 6(a) reveals the extinction spectra of single Au NP with the diameter D ranged from 40 nm to 80 nm, the dipole surface plasmon resonances range from 420 nm to 530 nm, which gravely deviates from the experimental results. Therefore, the absorption peak shown in Fig. 5(b) cannot be obtained from isolated Au nanoparticles definitely. To account for these features of our experiments, dimers of Au NPs simulations were performed and shown in Fig. 6(b). It indicates that surface plasmon resonances located around 600 nm can be obtained. Therefore, dimers can be responsible for the absorption spectra of Au NPs. Fig. 6(c) demonstrates the electric field distributions of isolated and dimer of Au NPs. Plasmon coupling in the dimers of metal NPs dependence of their distances could modulate the dipole surface plasmon resonances. Further, plasmon coupling would influence the absorption and release energy of gold nanoparticles[14,17,19,51]. Therefore, the size, shape and composition of the plasmonic nanostructures can be adapted to obtain broad absorption[6,11,18,52].

Radiative recombination in Au NPs has been observed arising from transitions between electrons in conduction-band states below the Fermi level and holes in the d bands generated by optical excitation[17,19,20,53]. The excitation process relies on the size of nanopaticles, the environment materials that surround the particle, as well as the plasmon coupling induced by the distances among nanoparticles[19,50]. This emission roots in the transition between the states near the Fermi energy, in contrast to the excited holes in the deep-lying bands. The luminescence derived from the decay radiatively via re-emitted photons can be interpreted in terms of light scattering which involved surface roughness and which showed zero intensity for emission normal to the surface. The dependence of the peak emission wavelength on Au NPs was consistent with the surface plasmon resonance. The luminescence was excited due to the EL from ZnO MWs (500 nm). Following light absorption and local surface plasmon resonances excitation in these hybridized plasmonic structures, electromagnetic decay takes place, radiatively through re-emitted photons shown in Fig. 7(a). As we mentioned above, the dimer of Au NPs is responsible for the localized surface plasmon resonances around 600 nm, therefore, localized surface plasmon resonance modes can be split into two kinds: the bright mode can be derived from electrically driven surface defect excitation, and the dark mode can be derived from the near field coupling interaction among Au NPs shown in Fig. 6(c). The plasmon coupling among dimers guarantees that there is almost no wavelength shift. Simultaneously, the dark modes appeared causes the intraband transition of NPs, and then forms the radiation loss, as shown in Fig. 7(b). Localized surface plasmon induced PL of Au NPs is generally considered to be a process that electrons from the occupied d bands are first excited by 520 nm pumped, the absorption leads to unoccupied states of the sp-conduction band. Then, subsequent intraband scattering processes prompts the electrons relaxation to the Fermi level. Eventually, the relaxation of the electron-hole pair recombines either through nonradiative processes, or by means of the emission of luminescence. Radiative relaxation energies are therefore strongly connected to the interband separation. For the case of small particles where the optical properties are dominated by localized surface plasmon resonances, PL spectra can be observed, suggesting that the photoemission is related to the surface plasmons[16,17,20,36,47,48].

The electronic energy will transfer from MWs to metal surface within the distance less than 10 nm in a non-radiative process, and the efficiency is inversely proportional to the third power of the distance[54]. In the experimental, the Au NPs sputtered on the surfaces of MWs, therefore, the Au NPs are in direct contact with ZnO MWs. In the contact areas of Au NPs coated ZnO MWs, the radiatively status would be suppressed, and then transitions to be the non-radiative process. Non-radiative decay in noble-metal nanostructures can take place through intraband excitations within the conduction

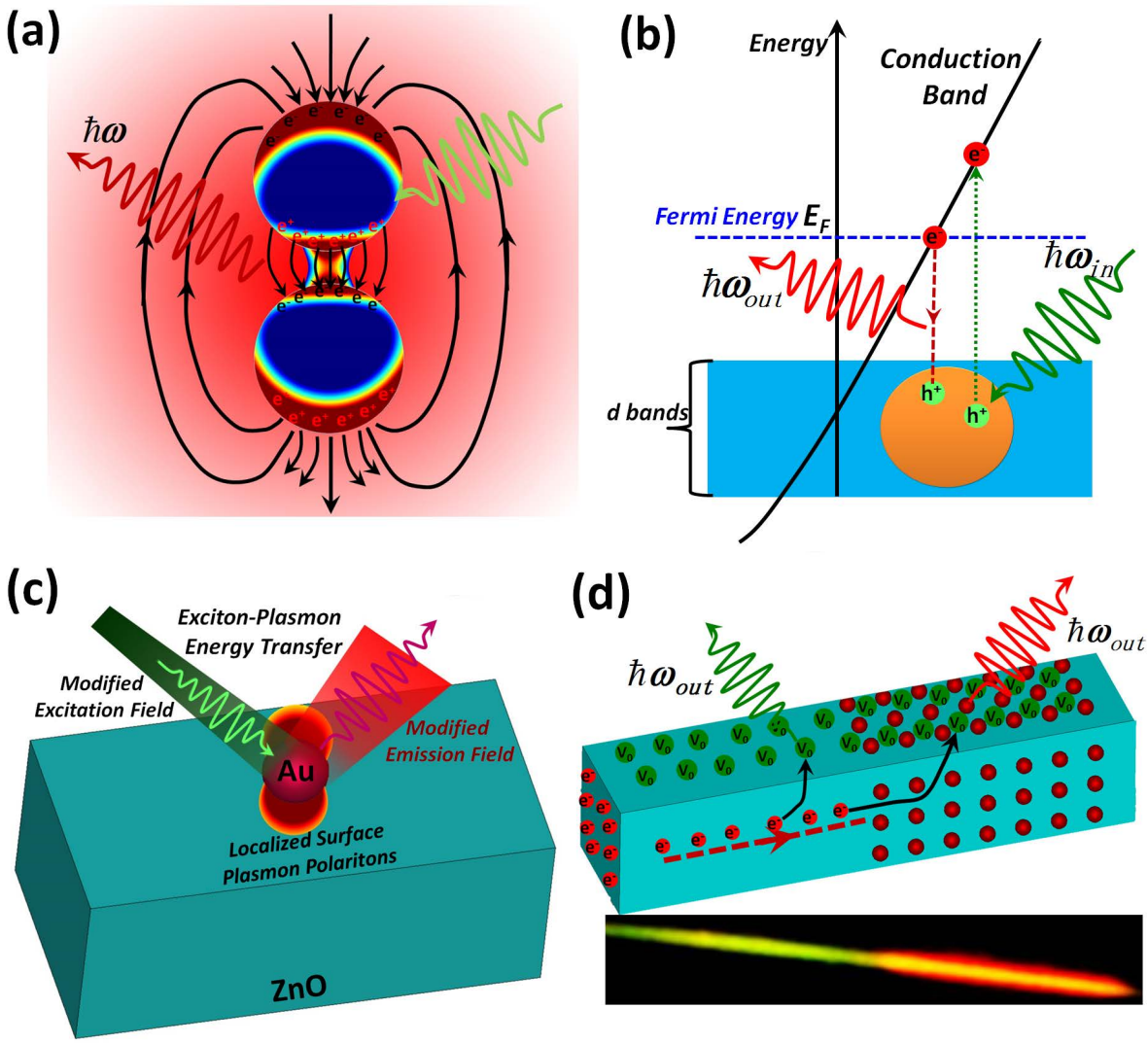

Fig. 7 Excitation and recombination mechanisms of Au nanoparticles: (a) Localized surface plasmons of Au dimers can decay radiatively via re-emitted photons; (b)Schematic band structure of Au nanoparticles showing the excitation and recombination transitions; (c) Schematic of resonant exciton-plasmon interactions that can occur in metal-semiconductor hybridized plasmonic structures; (d) Electrically driven induces the electron transport process, which reveals surface defect modes excitation of bare ZnO microwire, and the plasmon assisted enhancement and suppression mechanisms on the basis of Au nanoparticles coated ZnO microwire.

band, or through interband excitations caused by transitions between other *d* bands and the conduction band (The corresponding radiation process can be referred to Fig. 4). The *d* band energy levels lie 2.4 eV below the Fermi energy levels for Au, making interband excitations considerably more unlikely than intraband excitations[13,15,19,21,50]. Fig. 7(b) depicts the parabolic conduction band of Au nanoparticle with a Fermi energy E_F. After non-radiative surface plasmon decay, electrons from occupied energy levels are excited above the Fermi energy. Localized surface plasmons in Au NPs can transfer energies between approximately 1 eV and 4 eV to hot electrons; this energy depends on the carrier concentration, the size and the shapes of the nanostructures shown in Fig. 7(c). After injection of hot electrons, the plasmonic nanostructures are left positively charged because of electronic depletion. An electron-donor solution or a hole-transporting materials is required to be in contact with the nanostructures, which can be used as carriers to transport the generated holes to the counter electrode, keeping the charge balance and sustaining an electric current. The further luminescence process

was demonstrated in Fig. 7(d), that is, the green emitting can be excited due to the bare ZnO microwire, while the red emitting can be excited due to the Au nanoparticles coated ZnO microwire. The inset reveals the corresponding dual emitting phenomenon[6,19,55].

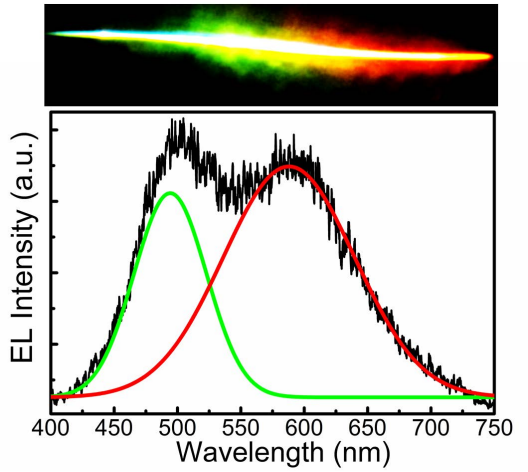

Fig. 8 Electroluminescence center fitting of surface defect modes based on the same ZnO microwire: the green line demonstrates the surface defects luminescence of bare ZnO microwire; the red line demonstrates plasmon mediated the other electroluminescence emitting process; the inset shows the camera images corresponding to the electroluminescence emitting along the microwire length direction.

To further demonstrate the excitation and recombination mechanisms, as shown in Fig. 7(d), the model was realized experimentally. Fig. 8 indicates the dual emissions processes. Two independent luminescence centers located around 500nm, and 600 nm respectively, can be observed simultaneously. The corresponding emitting phenomenon just with a camera in the microscope has been shown in the inset of Fig. 8. Plasmon mediated energy transfer process is based on the concept that Au NPs treated as an excited acceptor, such as an oscillating dipole that can undergo energy exchange with a dipole resonant emission, which has a similar resonance frequency. Au NPs absorb the energy released from the surface defects emission around 500 nm, provided a platform for the selective excitation of the localized surface plasmon resonances. Resonance energy transfer requires a spectral overlap between the donor emission and the acceptor absorbance spectra. In principle, if the surface plasmon resonance spectra of the Au NPs overlaps the luminescence spectrum of an acceptor molecule, and the donor can directly transfer its excitation energy to the acceptor via exchange of a virtual photon. Therefore, the coupling interaction between metal plasmons and excitons occurs, which can achieve the amplification of the emission. It is evident that there is no significant spectral overlap of the ZnO surface defects emission with the absorption spectra of Au nanoparticles shown in Figs. 4 and 5. In contrast the overlap between the exciton emission of ZnO and Au nanoparticles absorbance is negligible. The red emission center around 600 nm can be attributed to energy released from the Au NPs surface plasmon resonances[20,37,43]. In addition, metal photoluminescence originated from radiative recombination of photoexcited core holes and conduction band electrons has been confirmed[15,19,20]. Au nanoparticles surface plasmon local field effect can induce the enhancement of metal photoluminescence. Localized surface plasmons can decay radiatively via re-emitted photons, or non-radiatively via a excitation of hot electrons. Therefore, both plasmon assisted enhancement and suppression mechanisms can be realized by means of the radiative recombination in Au nanoparticles arising from the transitions between electrons in conduction-band states below the Fermi level and holes in the *d* bands generated by optical excitation. In order to confirm that observed emission was not due to some other source such as Raman scattering from electrons, or Au plasmon-enhanced another surface

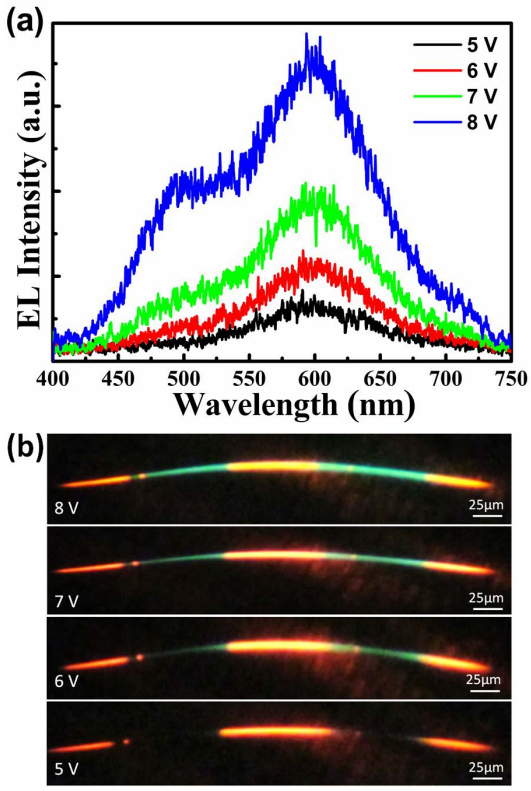

Fig. 9 Electroluminescence spectra based on the device of Fig. 1: (a) Electroluminescence spectra operated between 5 V and 8 V; (b) the camera images corresponding to the electroluminescence pattern along the microwire length direction under different electrical injection current.

defect electroluminescence, Au nanoparticle sputtered on part of ZnO microwires have been carried out, and found that red emitting can be obtained from the region of Au nanoparticles coated ZnO microwire shown in Fig. 8. Meanwhile, the others metal NPs, such as Ag, Pt, were also explored, nevertheless, the luminescence processes cannot be observed [10,53]. The present results are quite unambiguous, as well as no correction was taken into account for reabsorption in the present work.

The energy transfer process will be concentrated on in this section to display plasmon-assisted enhancement and suppression mechanisms. The devices based on a single ZnO microwire with Au NPs sputtered on partially were built, as shown in Fig. 1. The EL and luminescent images shown in Fig. 8 display dual emission excitation. The detailed process can be referred to the Fig. 9. Figure 9(a) shows the EL spectra with different injection currents. In the case of small current injection, only the red emitting and the corresponding 600 nm luminescent centers can be observed. Once the incident current increasing to a certain value, dual emissions excitation can be achieved. Therefore, Au NPs photoluminescence originated from radiative recombination of photoexcited core holes and conduction band electrons is enhanced owing to the surface plasmon local field effect. Simultaneously, the inhibition and amplification phenomenons induced by local surface plasmon resonance from 500 nm to 600 nm has been demonstrated explicitly. It can be found that the surface plasmons of Au NPs not only can enhance the radiative recombination of photoexcited core holes and conduction band electrons, but also maintain the energy release and transfer, and restrain the surface defects EL [16,20,47,48]. The investigation of detailed excitation and recombination mechanisms provides further evidences: firstly that Ohmic contact indicates the green emission is due to the surface defect modes, secondly that the introduction of Au nanoparticles not only can result in the ZnO defect state emission transfer, but also bring the suppression, and thirdly that the quenching originates from a single process, which can be ascribed to energy transfer [7,56].

4 Conclusion

Generally speaking, electrically driven plasmon mediated energy transfer between the surface defect modes of ZnO micrcowires and localized surface plasmon modes of Au NPs has been realized. Electrically driven green emitting has been obtained due to the V_O^+ defect states, which existed in the surface depletion region. By means of introducing Au nanoparticles, visible defect emission has been modified along with a red shift in Au@ZnO microwires system. Intraband transition of Au nanoparticles leads to the decay radiatively via reemitted photons, which is responsible for the red emitting. The excitation and recombination of the surface defect modes can be attributed to the dimers of Au NPs, which leaded to signal suppression or amplified under electrically driven. A direct application of the strategy outlined above would be to develop ZnO based light-emitting diodes. Another potential area of application is synthetic light harvesting and modulation structures; plasmonic modes could act to channel the energy transfer from absorbing species to reaction centers and more generally in photophysics near surfaces.

Acknowledgements

This work is supported by National Basic Research Program of China (973 Program) under Grant Nos. (2011CB302006, 2011CB302004), the Key Program of the National Natural Science Foundation of China (11134009), the National Natural Science Foundation of China under Grant Nos. (11404328, 21101146) the 100 Talents Program of the Chinese Academy of Sciences.

References

1 M. Lunz, X. Zhang, V. A. Gerard, Y. K. Gunko, V. Lesnyak, N. Gaponik, A. S. Susha, A. L. Rogach and A. L. Bradley, *J. Phys. Chem. C*, 2012, **116**, 26529–26534.
2 X. Zhang, C. A. Marocico, M. Lunz, V. A. Gerard, Y. K. Gunko, V. Lesnyak, N. Gaponik, A. S. Susha, A. L. Rogach and A. L. Bradley, *ACS Nano*, 2014, **8**, 1273–1283.
3 K. A. Velizhanin and T. V. Shahbazyan, *Phys. Rev. B*, 2012, **86**, 245432.
4 C. Zhang, M. L. F. Lerch, A. D. Martin, P. E. Simmonds and L. Eaves, *Phys. Rev. Lett.*, 1994, **72**, 3397–3400.
5 P. Andrew and W. L. Barnes, *Science*, 2000, **290**, 785–788.
6 V. N. Pustovit and T. V. Shahbazyan, *Phys. Rev. B*, 2011, **83**, 085427.
7 X. Zhang, C. A. Marocico, M. Lunz, V. A. Gerard, Y. K. Gunko, V. Lesnyak, N. Gaponik, A. S. Susha, A. L. Rogach and A. L. Bradley, *ACS Nano*, 2014, **8**, 1273–1283.
8 P. Andrew and W. L. Barnes, *Science*, 2004, **306**, 1002–1005.
9 M.-M. Jiang, H.-Y. Chen, C.-X. Shan and D.-Z. Shen, *Phys. Chem. Chem. Phys.*, 2014, **16**, 16233–16240.
10 B. P. Khanal, A. Pandey, L. Li, Q. Lin, W. K. Bae, H. Luo, V. I. Klimov and J. M. Pietryga, *ACS Nano*, 2012, **6**, 3832–3840.
11 V. Karanikolas, C. A. Marocico and A. L. Bradley, *Phys. Rev. A*, 2014, **89**, 063817.
12 R. Hildner, D. Brinks, J. B. Nieder, R. J. Cogdell and N. F. van Hulst, *Science*, 2013, **340**, 1448–1451.
13 C. Clavero, *Nat. Photon.*, 2014, **8**, 95–103.
14 X. Fan, W. Zheng and D. J. Singh, *Light: Sci. Appl.*, 2014, **3**, e179.
15 M. Achermann, *J. Phys. Chem. Lett.*, 2010, **1**, 2837–2843.
16 H. Hu, H. Duan, J. K. Yang and Z. X. Shen, *ACS Nano*, 2012, **6**, 10147–10155.
17 E. Dulkeith, T. Niedereichholz, T. A. Klar, J. Feldmann, G. von Plessen, D. I. Gittins, K. S. Mayya and F. Caruso, *Phys. Rev. B*, 2004, **70**, 205424.
18 G. Schatz, *J. Phys. Chem. Lett.*, 2010, **1**, 2980–2981.
19 A. Mooradian, *Phys. Rev. Lett.*, 1969, **22**, 185–187.
20 T. V. Shahbazyan, *Nano Lett.*, 2013, **13**, 194–198.
21 Y.-Y. Lai, Y.-P. Lan and T.-C. Lu, *Light: Sci. Appl.*, 2013, **2**, e76.
22 E. Matioli, S. Brinkley, K. M. Kelchner, Y.-L. Hu, S. Nakamura, S. DenBaars, J. Speck and C. Weisbuch, *Light: Sci. Appl.*, 2012, **1**, e22.
23 C. Ton-That, L. Weston and M. R. Phillips, *Phys. Rev. B*, 2012, **86**, 115205.

24 A. Alkauskas, J. L. Lyons, D. Steiauf and C. G. Van de Walle, *Phys. Rev. Lett.*, 2012, **109**, 267401.

25 M. R. Wagner, G. Callsen, J. S. Reparaz, J.-H. Schulze, R. Kirste, M. Cobet, I. A. Ostapenko, S. Rodt, C. Nenstiel, M. Kaiser, A. Hoffmann, A. V. Rodina, M. R. Phillips, S. Lautenschläger, S. Eisermann and B. K. Meyer, *Phys. Rev. B*, 2011, **84**, 035313.

26 R. Vidya, P. Ravindran, H. Fjellvåg, B. G. Svensson, E. Monakhov, M. Ganchenkova and R. M. Nieminen, *Phys. Rev. B*, 2011, **83**, 045206.

27 A. Janotti and C. G. Van de Walle, *Phys. Rev. B*, 2007, **76**, 165202.

28 A. F. Kohan, G. Ceder, D. Morgan and C. G. Van de Walle, *Phys. Rev. B*, 2000, **61**, 15019–15027.

29 S. B. Zhang, S.-H. Wei and A. Zunger, *Phys. Rev. B*, 2001, **63**, 075205.

30 F. Stavale, L. Pascua, N. Nilius and H.-J. Freund, *J. Phys. Chem. C*, 2014, **118**, 13693–13696.

31 H. Y. Lin, C. L. Cheng, Y. Y. Chou, L. L. Huang, Y. F. Chen and K. T. Tsen, *Opt. Express*, 2006, **14**, 2372–2379.

32 S. T. Kochuveedu, J. H. Oh, Y. R. Do and D. H. Kim, *Chem. Eur. J.*, 2012, **18**, 7467–7472.

33 C.-S. Wang, H.-Y. Lin, J.-M. Lin and Y.-F. Chen, *Applied Physics Express*, 2012, **5**, 062003.

34 Y.-M. Chang, M.-L. Lin, T.-Y. Lai, H.-Y. Lee, C.-M. Lin, Y.-C. S. Wu and J.-Y. Juang, *ACS Appl. Mater. Interfaces*, 2012, **4**, 6676–6682.

35 C. F. Guo, T. Sun, F. Cao, Q. Liu and Z. Ren, *Light: Sci. Appl.*, 2014, **3**, e161.

36 S. T. Kochuveedu and D. H. Kim, *Nanoscale*, 2014, **6**, 4966–4984.

37 M. Achermann, *J. Phys. Chem. Lett.*, 2010, **1**, 2837–2843.

38 H. Guo, Z. Lin, Z. Feng, L. Lin and J. Zhou, *J. Phys. Chem. C*, 2009, **113**, 12546–12550.

39 C.-H. Chen, S.-J. Chang, S.-P. Chang, M.-J. Li, I.-C. Chen, T.-J. Hsueh, A.-D. Hsu and C.-L. Hsu, *J. Phys. Chem. C*, 2010, **114**, 12422–12426.

40 A. J. Morfa, B. C. Gibson, M. Karg, T. J. Karle, A. D. Greentree, P. Mulvaney and S. Tomljenovic-Hanic, *Nano Lett*, 2012, **12**, 949–954.

41 G. A. Beane, A. J. Morfa, A. M. Funston and P. Mulvaney, *J. Phys. Chem. C*, 2012, **116**, 3305–3310.

42 A. J. Morfa, N. Kirkwood, M. Karg, T. B. Singh and P. Mulvaney, *J. Phys. Chem. C*, 2011, **115**, 8312–8315.

43 Z.-M. Liao, H.-Z. Zhang, Y.-B. Zhou, J. Xu, J.-M. Zhang and D.-P. Yu, *Phys. Lett. A*, 2008, **372**, 4505 – 4509.

44 M.-M. Jiang, B. Zhao, H.-Y. Chen, D.-X. Zhao, C.-X. Shan and D.-Z. Shen, *Nanoscale*, 2014, **6**, 1354–1361.

45 C.-Y. Chen, J. R. D. Retamal, I.-W. Wu, D.-H. Lien, M.-W. Chen, Y. Ding, Y.-L. Chueh, C.-I. Wu and J.-H. He, *ACS Nano*, 2012, **6**, 9366–9372.

46 M. Ding, D. Zhao, B. Yao, B. Li, Z. Zhang, C. Shan and D. Shen, *J. Phys. D: Appl. Phys.*, 2011, **44**, 075104.

47 A. Bouhelier, R. Bachelot, G. Lerondel, S. Kostcheev, P. Royer and G. Wiederrecht, *Phys. Rev. Lett.*, 2005, **95**, 267405.

48 E. Dulkeith, T. Niedereichholz, T. Klar, J. Feldmann, G. Von Plessen, D. Gittins, K. Mayya and F. Caruso, *Phys. Rev. B*, 2004, **70**, 205424.

49 P. B. Johnson and R. W. Christy, *Phys. Rev. B*, 1972, **6**, 4370–4379.

50 B. M. Reinhard, M. Siu, H. Agarwal, A. P. Alivisatos and J. Liphardt, *Nano Lett.*, 2005, **5**, 2246–2252.

51 N. J. Halas, S. Lal, W.-S. Chang, S. Link and P. Nordlander, *Chem. Rev.*, 2011, **111**, 3913–3961.

52 X. Wu, Y. Xiao, C. Meng, X. Zhang, S. Yu, Y. Wang, C. Yang, X. Guo, C.-Z. Ning and L. Tong, *Nano Lett.*, 2013, **13**, 5654–5659.

53 M. R. Beversluis, A. Bouhelier and L. Novotny, *Phys. Rev. B*, 2003, **68**, 115433.

54 A. Campion, A. Gallo, C. Harris, H. Robota and P. Whitmore, *Chem. Phys. Lett.*, 1980, **73**, 447–450.

55 J. Zheng, C. Zhou, M. Yu and J. Liu, *Nanoscale*, 2012, **4**, 4073–4083.

56 E. Khon, A. Mereshchenko, A. N. Tarnovsky, K. Acharya, A. Klinkova, N. N. Hewa-Kasakarage, I. Nemitz and M. Zamkov, *Nano Lett.*, 2011, **11**, 1792–1799.